

A 1-gram dual sensorless speed governor for micro-air vehicles

S. Viollet, *Member, IEEE*, L. Kerhuel and N. Franceschini

Abstract—Embedding electronic control circuits onboard micro-air vehicles (MAVs) is a challenge in view of the stringent limitations in terms of mass, size, and power consumption. The propulsion unit is a cornerstone in the design of a MAV. In this study, we introduce a ‘sensorless’ speed governor (regulator) for a propulsion unit composed of a miniature propeller (diameter 12cm), a reduction gear, and a 8-gram coreless DC motor. In contrast with classical electronic speed controllers (ESC) designed for model aircraft, our speed governor operates in a closed-loop mode. Yet it does not require any tachogenerator. Experimental results show that our control strategy exhibits four main advantages:

- it makes the rotor speed swiftly attain any new velocity set-point.
- it makes the rotor speed virtually insensitive to aerodynamical (gusts) disturbances.
- it makes the rotor speed largely insensitive to the drop in battery supply voltage.
- it makes the yaw autopilot of a miniature aerial robot act as a yaw damper.

The two-channel speed regulator that we designed and built is used to servo the rotational speed of two propellers independently, without the need for any mechanical or optical tachometers. A new generation digital signal controller (dsPIC) allowed us to make this two-channel speed regulator small (13x15mm), lightweight (1g) and fully compatible with the 100-gram OSCAR II aerial robot developed at our laboratory.

I. INTRODUCTION

Due to its simplicity of control, the DC motor is still a first choice for actuating robotic platforms. Recent studies have shown that DC motors are well suited to generate the lift and thrust required by miniature aerial robots [1], [2], [3], [4], [5], [6], [7], [8]. Developing a micro air vehicle represents a big challenge in terms of size and mass of the embedded electronics [1], [5]. This calls for solutions that simplify mechanical assemblies and reduce the size of electronic circuits. In this context, the sensorless control of actuators (micromotors, piezo actuators, etc.) allows to benefit from the favorable properties of a feedback system (in terms of disturbance rejection, improved accuracy, improved dynamics, etc.) without the need for any modification in the mechanical design of the robot. Several examples of integrated-circuits based [9], microcontroller based [10], [11], [12], [13], or DSP based [14] sensorless speed regulators for DC motors can be found in the literature. However, few examples of a sensorless control system for a propulsion unit can be found in the autonomous aerial robotic field. Most off-the-shelf electronic speed controllers (ESC), designed for model

aircraft equipped with brushed or brushless DC motors, are not aimed at maintaining the rotor speed constant (i.e., at operating in the ‘governor mode’) when the propeller drive is subjected to electrical and/or aerodynamical disturbances. The need for feedback control in a propulsion group is crucial. Flying robots, whether based on fixed or rotatory wings, are subject to severe disturbances:

- aerodynamical disturbances (ground effects, wind gusts, etc.). Sensitivity to such disturbances increases with blade rigidity.
- electrical disturbances (gradual battery voltage decrease).
- nonlinear dynamics introduced by the propeller, rotor or thruster.

In model helicopters, the use of rotor speed as a control variable is liable to introduce nonlinearities that will complicate the rotorcraft’s closed-loop control [15]. This is why holding the rotor speed constant is paramount to the design of an attitude controller. Likewise, in underwater autonomous vehicles (UAVs), electrically powered UAV can become unstable if the dynamical characteristics of the thrusters are neglected in the control system design [16].

Given that the few ESC available that include a governor mode are bulky and heavy, we describe here the implementation of a miniature sensorless speed regulator dedicated to the control of a propulsion group based on a miniature coreless DC motor. Our regulator requires simply that the armature voltage and the motor current be measured. Recent studies [12], [13] have shown the reliability of PIC micro-controllers in motor speed control systems. A new generation of digital signal controller (dsPIC from Microchip), which is a hybrid chip incorporating both a micro-controller unit (MCU) and a DSP, allowed us to perform the speed regulation of two micromotors independently with the same MCU, thanks to the integration of many peripherals (PWM, ADC). In section 2, we describe how the motor speed is estimated. We also describe the rapid prototyping tool used to implement the sensorless speed regulator from the Simulink graphical environment to the dsPIC. Experimental results are given in section 3 where we assess the performances of the regulator in terms of its step response and disturbance rejection. Section 4 highlights the beneficial effect of rotor speed regulation on the closed-loop behavior of a newly designed twin-engine aerial robot, OSCAR II [17].

S. Viollet, L. Kerhuel and N. Franceschini are with the Biorobotics Dept. at the Institute of the Movement Sciences, CNRS/Univ de la Méditerranée, CP 938, 163, avenue de Luminy, 13288 Marseille Cedex 09, France (email: stephane.viollet, lubin.kerhuel, nicolas.franceschini@univmed.fr)

II. IMPLEMENTATION OF THE SENSORLESS SPEED REGULATOR

A. Structure of the electronic circuit

The miniature DC motors (power 7W, mass 8g) used in this study originates from the tail rotor of a model helicopter. The maximum allowable current drawn is 900mA under 7.2V. The motor is loaded by a light (0.8 gram) two-blade propeller (diameter 12cm) mounted on the output shaft, via a 5:1 reduction gear.

Figure 1 shows the closed-loop control scheme of the speed regulator based on the estimation of the rotor speed.

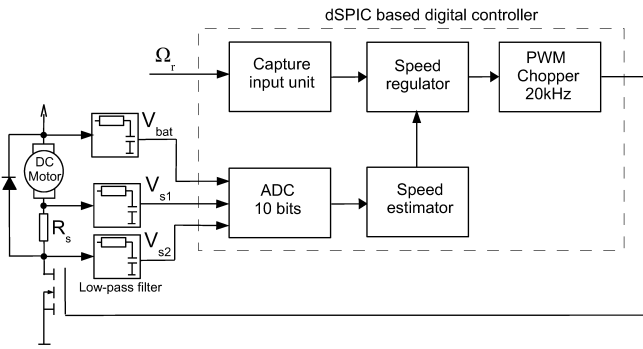


Fig. 1. Diagram of the sensorless speed regulator. The motor speed is estimated from the measurement of the armature voltage ($V_{bat} - V_{s1}$) and from the current flowing through an additional shunt resistor R_s .

B. Estimation of the rotor speed

The dynamics of a DC motor is described by the following equations

$$J_m \frac{d\Omega_m}{dt} + b\Omega_m = K_t i_m + T_l \quad (1)$$

$$K_e \Omega_m + L_m \frac{di_m}{dt} + R_m i_m = v_a \quad (2)$$

with rotor speed Ω_m , viscous friction coefficient b , rotor inertia J_m , terminal resistance R_m , rotor inductance L_m , torque constant K_t , back EMF constant K_e , armature voltage v_a , motor current i_m and load-torque T_l . Applying Laplace transform to equations (1) and (2) yields

$$sJ_m \Omega_m + b\Omega_m(s) = K_t I_m(s) + T_l(s) \quad (3)$$

$$K_e \Omega_m(s) + sL_m I_m(s) + R_m I_m(s) = V_a(s) \quad (4)$$

As depicted in figure 1, the armature voltage V_a of the motor is defined by

$$V_a = V_{bat} - V_{s1} \quad (5)$$

and the motor current I_m is measured through the shunt resistor R_s and a gain k

$$I_m = (V_{s1} - V_{s2}) / (kR_s) \quad (6)$$

The estimated rotor speed Ω_e is calculated by applying

$$K_{est} \Omega_e = [V_a - (V_{s1} - V_{s2})] F(s) = [V_a - kR_s I_m(s)] F(s) \quad (7)$$

with $F(s) = 1/(1 + \tau_f s)$, the low-pass filter of the V_{bat} , V_{s1} and V_{s2} signals (see Fig. 1).

Applying (4) and (6) to (7) and considering the inductance L_m small leads to

$$K_{est} \Omega_e = [(R_m - kR_s) I_m(s) + K_e \Omega_m(s)] F(s) \quad (8)$$

From (3), if we consider the load-torque T_l null, the transfer function between the motor current I_m and the rotor speed Ω_m is given by

$$\frac{I_m(s)}{\Omega_m(s)} = \frac{(J_m s + b)}{K_t} \quad (9)$$

Applying (9) to (8), considering that $K_e = K_t$ and b small leads to

$$\Omega_e(s) = \frac{K_e}{K_{est}} (1 + \tau s) F(s) \Omega_m(s) \quad (10)$$

From (10), if we choose $K_{est} = K_e$, we have

$$\Omega_e(s) = \frac{(1 + \tau s)}{(1 + \tau_f s)} \Omega_m(s) \quad (11)$$

with $\tau = ((R_m - kR_s) J_m) / K_e^2$.

The expression of τ shows that the values of the shunt resistor and the current gain k are critical. Indeed, if we choose the current gain k such that kR_s becomes higher than R_m , the estimator given in (11) leads to a nonminimum-phase system which can cause initial undershoot. As shown in [18], open-half-right-planes zeros must be avoided due to the limit that they would impose upon the bandwidth. Then, the value of the current gain k must therefore be set by taking into account the value of the terminal resistance R_m and its possible variation due to the temperature.

From (11), if we choose k such that the shunt resistance kR_s becomes equal to the terminal resistance R_m , we make the estimated rotor speed Ω_e proportional to the motor speed Ω_m . Figure 2 shows the block diagram of the velocity feedback control system based on the estimation of the rotor speed. The estimated speed Ω_e is compared to the input reference Ω_r . The resulting speed error drives a digital proportional-integrator (PI) compensator which ensures zero steady-state error. The sampling frequency of the digital controller is equal to 10kHz. This high sampling frequency was reached by using fixed-point processing.

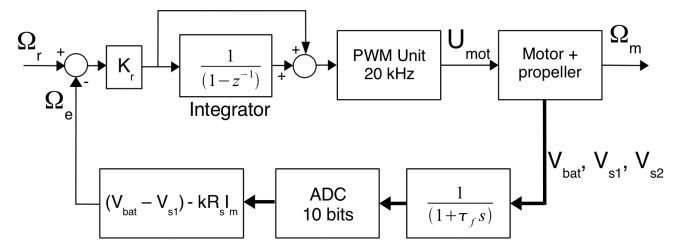


Fig. 2. Block diagram of the sensorless speed regulator. All processing steps (estimation of the motor's speed Ω_e and error integration) are achieved at a sampling period of 100 μ s.

As shown in figure 2, the input reference Ω_r is captured by the input capture unit of the dsPIC. The motor rotational

speed value is adjusted by a Pulse Width Modulation (PWM) signal Ω_r . Maximum speed is reached for a 1ms pulse width and minimum rotational speed is reached for a 0.02ms pulse, which makes the governor easily compatible with any standard radio control (R/C) receiver. In this study, however, we set the refresh rate of the PWM reference input Ω_r at 500Hz, which is 10-fold the refresh rate used in conventional radio-controlled models. Once introduced into a high level control system (e.g., an attitude autopilot system), our speed regulator therefore introduces a delay which is 10 times smaller than the one introduced in classical R/C devices.

The size of the circuit was reduced to its minimum (see figure 3) by using a new generation of micro-controller (dsPIC from Microchip), which offers two main advantages:

- it includes all the peripherals required for motor control (PWM, ADC and IC). The number of external electronic devices is therefore reduced considerably.
- it includes a 16-bit hardware multiplier. The processing time needed for the signal processing operations is therefore dramatically reduced.

We decided to use the Microchip dsPIC 30F2010 (running at 10Mhz), due to its very small size (5x5mm). For each motor, all the measurements V_{bat} , V_{s1} and V_{s2} are digitized by the integrated analog-to-digital converter (6 channels, 10-bit resolution, maximum sampling rate of 1000 kilo-samples per second). The supply voltage V_{bat} is common to the two motors.

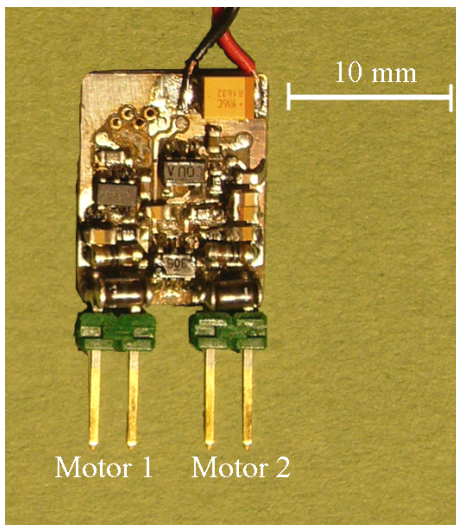


Fig. 3. Top view of the 1-gram, dual channel sensorless speed regulator. The back side is mainly occupied by the dsPIC (size 5x5mm). The device requires only two pulse-based (0-1ms width) input signals (not shown here) for setting the rotational speed of each motor independently.

C. Fast implementation with a rapid prototyping tool

During the implementation phase, this sensorless speed regulator served as a genuine test bench for testing the reliability of our custom-made rapid control prototyping toolbox for dsPIC [19]. We developed a complete tool to program

the Microchip embedded digital controller directly from the Mathworks (Simulink, Real Time Workshop) environment (cf. figure 4), without typing any C code lines. This novel *automatic code generation tool* makes the implementation of a digital control system considerably easier and faster because:

- it generates and compiles bug-free C code
- it provides block-level access to on-chip peripherals
- it optimizes the size of the C code
- it enables fixed-point system design, simulation and scaling.

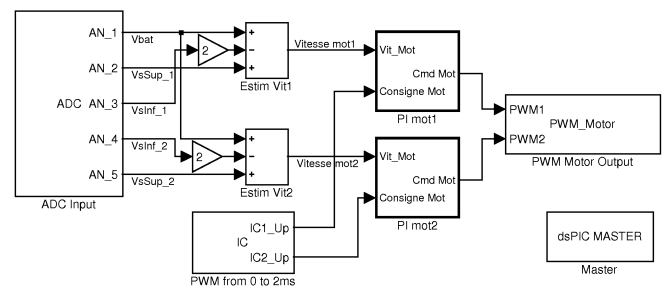


Fig. 4. Rapid prototyping of the sensorless speed regulator. With custom-made push-button automation, C code is generated directly from the block diagram under Simulink environment, compiled and downloaded into the dsPIC target [19].

Table 1 shows the main characteristics of the sensorless speed governor in its 'low power' and 'high power' version (not described here).

	Low power	High power (not shown)
Size	13x15mm	13x25mm
Mass (including 0.5g connectors)	1g	1.5g
Supply voltage	5,3V (min) 16V (max)	idem
Supply current (motors off)	40mA (under 7.2V)	idem
Current max (per channel under 8V)	2A	5A

TABLE I
MAIN CHARACTERISTICS OF THE SPEED REGULATOR

III. PERFORMANCES

A. Response time enhancement

To assess the performances of the sensorless speed regulator, we compared the step responses of the propeller with and without the speed regulator at work:

- 'governor mode OFF' means that the PWM unit is driven directly by the input reference (i.e., $\Omega_r = U_{mot}$).
- 'governor mode ON' means that the PWM unit is driven at the speed input reference Ω_r through the speed feedback control system (Fig.2).

Figure 5 shows the response of the propeller to a step of speed of 900 rpm (i.e., 15 rotations per second, *rps*).

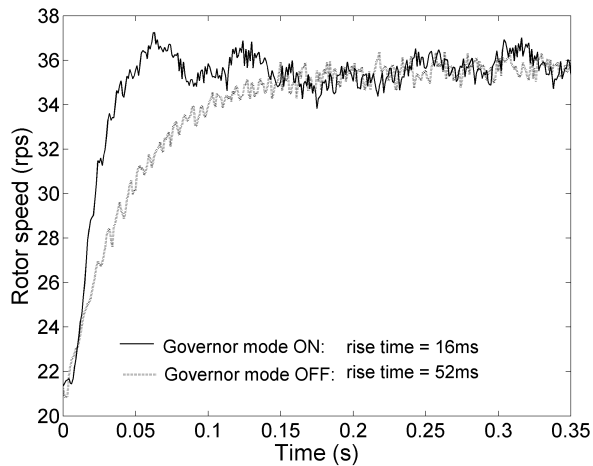


Fig. 5. Speed rise of the propeller shaft in response to a 15rps (i.e., 900 rpm) step input. With the governor mode set to OFF, the input reference Ω_r was sent directly to the PWM unit. $k = 1$, $K_r = 1.5$, $R_s = R_m = 1\Omega$ and $\tau_f = 2.3ms$.

Monitoring the actual rotational speed of the propeller was achieved by mounting onto the propeller shaft a light optical encoding disk (36 pulses per rotation) extracted from a computer mouse. Figure 5 shows the benefit of the sensorless control of the rotor speed in its ability to improve the dynamics by decreasing the rise time markedly (about 3-fold from 52ms down to 16ms). For a miniature aerial vehicle, setting a fast dynamics of the propeller is a critical issue because it is germane to a high reactivity. The latter is highly sought for in the context of daunting behaviours such as obstacle avoidance, hover flight and evasive manoeuvres.

B. Insensitivity to aerodynamical disturbances

Another benefit concerns the capability of the speed regulator to reject aerodynamic disturbances. To compare the response of the propeller with the governor mode set to either OFF or ON, we designed a wind gust generator by using an electric ducted fan (diameter 50mm) that was made to suddenly blow into the propeller (figure 6). An air valve was placed between the rotating propeller and the ducted fan (generating a steady wind). The propeller was rotating at an angular speed imposed by the value of Ω_r . The valve mounted onto the shaft of a servomotor introduced a sudden wind perturbation. Applying 45° rotational steps to the air valve (alternatively clockwise and counter-clockwise), we were able to change the speed of the headwind from 0 to $1m.s^{-1}$ in a very short time (60ms). Applying a series of periodic perturbation steps of this kind, (each lasting 2.5s), we measured the variation in rotor speed caused by this major perturbation (figure 7). Figure 7 shows that when the governor mode is set to OFF, the rotor speed is markedly affected by the gust of wind. Under closed loop conditions, by contrast, the periodic perturbations applied to the propeller are effectively compensated for.

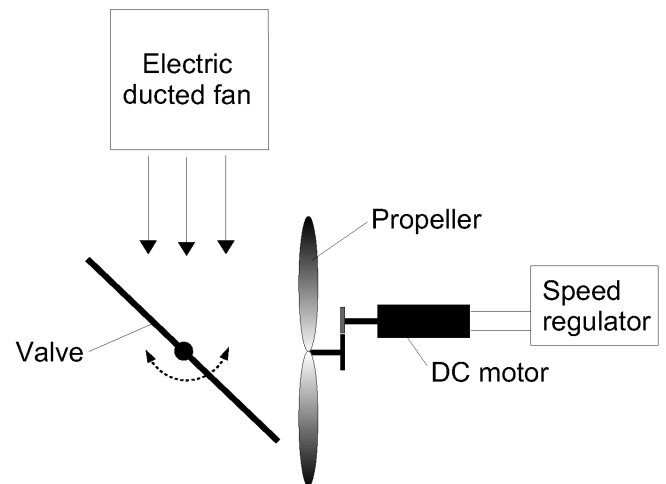


Fig. 6. Setup used for testing the performances of the sensorless speed regulator in its ability to compensate for aerodynamic perturbations (here a strong gust of wind). A wind-reflecting air valve was mounted onto a fast servomotor. The valve was suddenly rotated counterclockwise by 45° , thus directing the airflow into the propeller and causing a step of headwind at $1m.s^{-1}$.

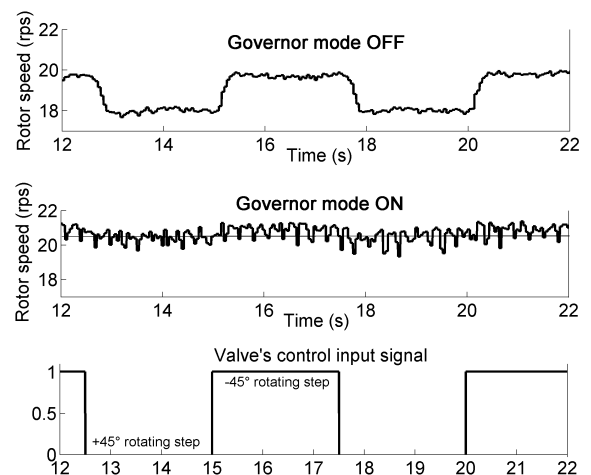


Fig. 7. Series of aerodynamic perturbations (gust of wind at $1m.s^{-1}$) applied to the turning propeller. With the governor turned off (top recording), the rotor speed is seen to be altered periodically. With the governor turned on (middle plot), the rotor speed can be seen to be virtually unaffected by the drastic wind gust and held relatively constant (mean value 20.6 rps). A positive ($+45^\circ$) rotational step corresponds to a counter-clockwise rotation applied to the valve (see figure 6).

C. Insensitivity to supply voltage variations

Figure 8 shows another major benefit of the speed regulator, namely its ability to compensate for the drop in battery supply voltage. The ability of the speed regulator to reject large supply voltage variations, avoids the need for adding a bulky DC-DC power regulator on-board the MAV, while permitting the flight time to be extended under nominal conditions.

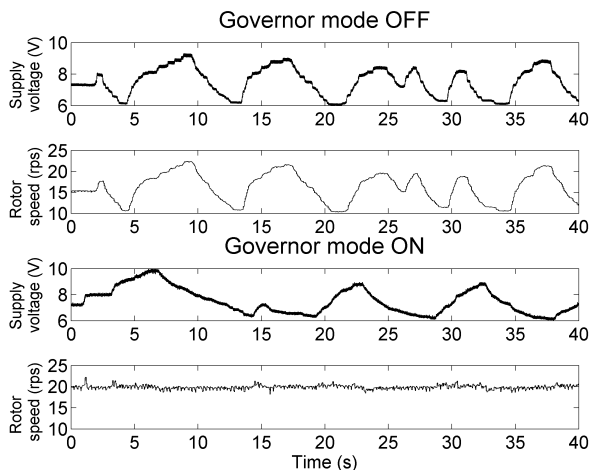


Fig. 8. Influence of changing the supply voltage upon the rotor speed in the ON and OFF modes. The supply voltage was changed manually. In the second case (governor mode turned ON), the propeller speed can be seen to be held virtually constant: the speed regulator virtually compensates for the large voltage perturbations.

IV. APPLICATION TO YAW ATTITUDE CONTROL OF A TWIN-ENGINE ROBOT

To illustrate the beneficial effect of having a speed regulator on each propeller axis, we mounted the 1-gram dual speed regulator onboard the miniature Oscar II robot shown in figure 9. Oscar II is a 100-gram aerial robot developed in our laboratory to test various visuomotor control strategies inspired by animals' sensorimotor reflexes [17]. Each propeller of the Oscar II robot is driven by a 8-gram DC micromotor connected to the sensorless speed regulator described above. For the following tests, attitude control of

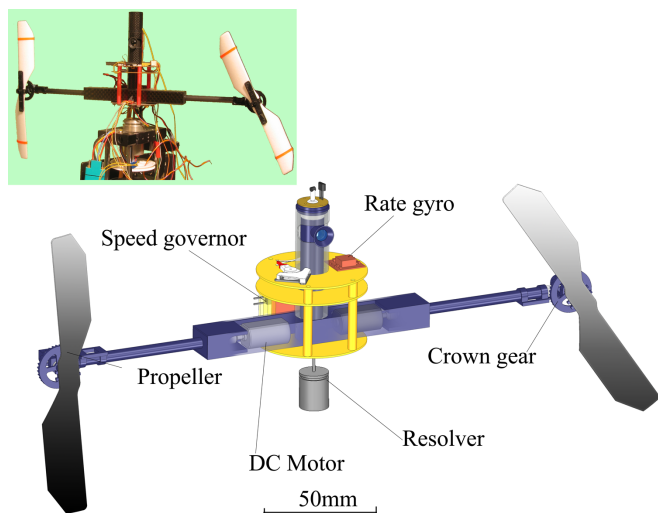


Fig. 9. The 100-gram Oscar II aerial robot controls its yaw turn visually by acting upon its two propellers differentially [17]. The two propulsion units are driven via the dual sensorless speed regulator described here, which acts as a speed governor for each propeller independently. The actual version of the robot is shown in the inset.

the robot about the yaw axis was achieved by implementing two feedback-loops as described in figure 10:

- an inner feedback-loop dealing with yaw angular speed. Yaw angular speed is measured with a micro rate-gyro (cf. figure 9).
- an outer feedback-loop dealing with yaw angular position. Yaw angular position is measured with a miniature resolver onto which the robot is mounted (Fig. 9).

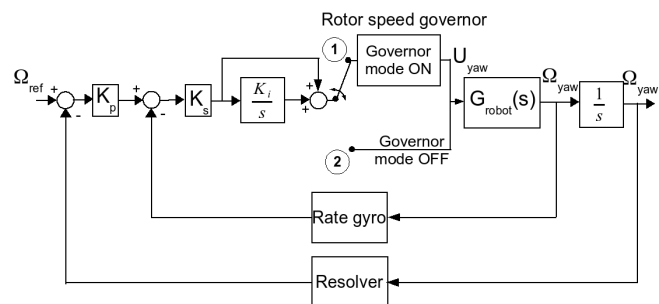


Fig. 10. Block diagram of the yaw attitude controller of the OSCAR II twin-engine aerial robot (figure 9). The aim of the experiment here is to compare the yaw step response of the robot with (switch position 1) and without (switch position 2) regulation of the rotor speed of each propeller. The yaw rate Ω_{yaw} is measured by a micro rate-gyro mounted on the robot's body and the yaw angular position Ψ_{yaw} is measured by a 12-bit resolver onto which the robot is mounted. $K_p = 8$, $K_s = 0.74$ and $K_i = 5$.

Figure 11 shows the robot's response to a large angular step displacement (25 degrees). The parameters (K_p , K_s and K_i) of the yaw attitude controller were identical in both cases. The difference in the two responses shown in figure 11 illustrates the conspicuous damping effect brought about by having the rotor speed of each propeller regulated locally. In the absence of rotor speed regulation (governor turned OFF) the robot follows the step but the response is largely underdamped (figure 11 dotted line). In the presence of rotor speed regulation (governor turned ON), the robot's yaw rotation appears to be markedly damped (figure 11 continuous line).

V. CONCLUSION

Prompted by the need to regulate the rotational speed of the propulsion units of a twin-engine micro aerial robot, we came to design and realize a miniature (13x15mm) and very light (1g) dual speed *sensorless* regulator. We described a simple way to regulate the rotational speed of a DC micromotor without adding the extra load of a dedicated (optical, magnetic or electro-mechanical) tachogenerator. The development of a rapid prototyping tool under MathWorks Simulink, combined with free development tools (Microchip) considerably decreased the time needed for the implementation of the digital control system onboard the robot. The relatively simple electronic design (based on few electronic devices) allows our speed regulator to be easily adapted to the wide power range of micromotors. An added advantage of the regulator is that it provides accurate monitoring of the supply voltage and rotor current. This feature is particularly useful

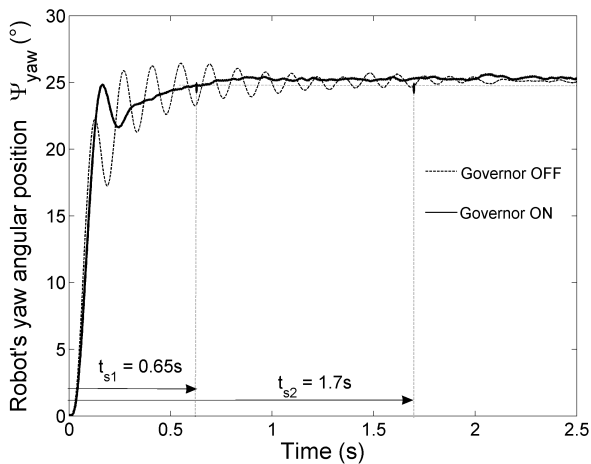


Fig. 11. Actual yaw response of the Oscar II aerial robot to a large angular step presented in two conditions: with the speed governor mode set to OFF (case 2 in figure 10) or ON (case 1 in figure 10). With the governor mode ON, the rise time remains unaltered but the settling time can be seen to be drastically reduced (about 2.5-fold, from 1.7s down to 0.65s). The yaw angular position Ψ_{yaw} was measured by the 12-bit resolver onto which the robot was mounted.

for preventing batteries (such as lithium-polymer batteries) from being damaged by an extended discharge, and for preventing the motor from being overrun, e.g., in case of an untimely shaft lock.

The sensorless speed governor may be of great advantage in the design of future micro-air vehicles. We showed that *local* servoing of each propeller speed introduced a significant yaw damping effect on the closed-loop behavior of our OSCAR II miniature aerial robot. The design of our sensorless speed regulator highlights the tight dependency of micro-aerial robotics upon integrated electronics.

ACKNOWLEDGEMENTS

We are very grateful to M. Boyron for his involvement in the electronic design. We thank F. Ruffier and J. Serres for fruitful discussions and comments on the manuscript. This work was supported by the French Research Agency (CNRS, Life science and Engineering science) and by the National Research Agency (ANR).

REFERENCES

- [1] J. Zufferey and D. Floreano, "Fly-inspired visual steering of an ultralight indoor aircraft," *IEEE Trans. on robotics*, vol. 50, pp. 177–194, 2006.
- [2] F. Ruffier and N. Franceschini, "Optic flow regulation: the key to aircraft automatic guidance," *Robotics and Autonomous Systems*, vol. 50, pp. 177–194, 2005.
- [3] P. Castillo, A. Dzul, and R. Lozano, "Real-time stabilization and tracking of a four rotor mini rotorcraft," *IEEE Transactions on Control Systems Technology*, vol. 12, pp. 510–516, 2004.
- [4] F. Ruffier, S. Viollet, and N. Franceschini, "Two autopilots based on insect vision for aerial robots," *Advanced Robotics*, vol. 18, pp. 771–786, 2004.
- [5] P. Pounds and R. Mahony, "Design of a four-rotor aerial robot," in *Australasian Conference on Robotics and Automation Conference*, 2002.

- [6] M. Ichikawa, H. Yamada, and J. Takeuchi, "Flying robot with biologically inspired vision," *Robotics and Mechatronics*, vol. 13, pp. 621–624, 2001.
- [7] S. Viollet and N. Franceschini, "Visual servo system based on a biologically-inspired scanning sensor," in *SPIE Conf. on Sensor fusion and decentralized control in Robotics II*, vol. 3839, 1999.
- [8] R. Mori, K. Hirata, and T. Kinoshita, "Vision-based guidance control of a small-scale unmanned helicopter," in *IEEE IROS*, 2007, pp. 2648–2653.
- [9] H. Sax, "How to drive dc motors with smart power ics," in *ST Microelectronics Application Note AN380*, 2003.
- [10] Z. Ahmad and M. N. Taib, "A study on the dc motor speed control by using back-emf voltage," in *IEEE Asian Conference on Sensors AsiaSense*, 2003, pp. 359–364.
- [11] B. Singh, J. R. P. Gupta, B. N. Singh, C. L. Puttaswamy, S. Gupta, and B. P. Singh, "Sliding mode control of a mechanical speed sensorless dc motor drive fed from a current controlled chopper," *Electric Power Components and Systems*, vol. 30, pp. 863–875, 2002.
- [12] M. Kim, J. Choi, J. Lee, H. Yoon, Y. Kim, and I. Cha, "A study on the dc motor speed control for electric bicycle with the load induction unit," in *IEEE Symp. On Industrial Electronics*, vol. 1, 2000, pp. 141–144.
- [13] B. S. Cunha, J. R. Camacho, and C. A. Bissochi, "Single-phase induction motor speed control through a pic controlled sinusoidal pwm inverter-the mathematical model and various load conditions," in *IEEE Int. Conf. on Power Tech*, 2001.
- [14] K. Ohishi, S. Matsuda, and K. Ohnishi, "Dsp-based dc servo acceleration control without speed sensor," in *IEEE IAS. Annual Meeting*, 1989, pp. 480–485.
- [15] M. van Nieuwstadt and J. C. Morris, "Control of rotor speed for a model helicopter: a design cycle," in *American Control Conference*, 1995, pp. 668–672.
- [16] D. Yoerger, J. Cooke, and J. J. Slotine, "The influence of thruster dynamics on underwater vehicle behavior and their incorporation into control system design," *IEEE J. of Oceanic Engineering*, vol. 15, pp. 167–178, 1990.
- [17] L. Kerhuel, S. Viollet, and N. Franceschini, "Sighted aerial robot with gaze and heading stabilization," in *IEEE IROS*, 2007, pp. 2634–2641.
- [18] J. B. Hoagg and D. S. Bernstein, "Nonminimum-phase zeros," *IEEE Control Systems magazine*, pp. 45–57, 2007.
- [19] L. Kerhuel. Embedded target for dspic. [Online]. Available: www.kerhuel.eu/RTWdsPIC